The role of kinetic asymmetry and power strokes in an information ratchet

DOI:
10.1016/j.chempr.2023.05.035

Document Version
Final published version

Chem

CellPress

Article

The role of kinetic asymmetry and power strokes in an information ratchet

Lorna Binks,[1] Stefan Borsley,[1] Todd R. Gingrich,[2] David A. Leigh,[1,*] Emanuele Penocchio,[2] and Benjamin M. W. Roberts[1]

[1]Department of Chemistry, University of Manchester M13 9PL, UK

[2]Department of Chemistry, Northwestern University, 2145 Sheridan Road, Evanston, IL 60208, USA

*Correspondence: david.leigh@manchester.ac.uk

SUMMARY

Biomolecular machines are driven by information ratchet mechanisms, where kinetic asymmetry in the machine's chemomechanical cycle of fuel-to-waste catalysis induces net directional dynamics. A large-scale energetically downhill conformational change, often termed a 'power stroke', has been erroneously implicated as a mechanistic driving feature in many such machines. We investigated the roles of kinetic asymmetry and power strokes in a series of minimalist rotaxane-based information ratchets with unsymmetrical equilibrium macrocycle distributions along the axle that lead to a power stroke (positive or negative) under fueling. We find that under chemical fueling kinetic asymmetry alone determines ratchet directionality, with all ratchets using the same amount of fuel to reach the same normalized steady state position. However, power strokes can nonetheless influence ratchet performance, such as how fast the ratchets reach the steady state. Moreover, nonequilibrium thermodynamic analysis reveals that the power stroke alters the amount and form (information/Shannon entropy versus inter-component binding energy) of free energy stored by the ratchet. These findings have implications for both the understanding of biological ratchets and the design principles for artificial nonequilibrium (supra)molecular machines.

Keywords: nonequilibrium chemistry, Brownian ratchets, molecular machines, rotaxanes, kinetic analysis, information thermodynamics.

THE BIGGER PICTURE

Biology uses autonomous molecular machines to power the essential processes of life. This nonequilibrium machinery is powered by chemical fuels such as ATP.

Minimalist artificial chemically fueled molecular machines have been developed, enabling the investigation of how structural features affect nonequilibrium dynamics.

The findings have significance for the understanding of fundamental biological processes and for the design of out-of-equilibrium molecular nanotechnology.

INTRODUCTION

The vital processes of life are mediated by complex molecular machinery,[1] transducing free energy[2] from their catalysis[3] of fuel-to-waste[4] to continuously and autonomously drive directional motion. Many of these biomachines appear to include a 'power stroke'[5,6] (that is, a large-scale, energetically downhill (co-)conformational change[7,8]) within their chemomechanical engine cycle.[3] Consequently, a 'power stroke mechanism' has often[5,6] been proposed to account

for the operation of such biomachines. This model posits that chemical steps raise the free energy of a motor, which then relaxes via the power stroke to move directionally,[6] reminiscent of the winding up and release of a macroscopic spring. While this imagery may be appealing from a macroscopic perspective (and has often been inappropriately used to describe the operation of biomolecular motors[5,6]), it has been convincingly shown[8–12] that ascribing the power stroke special significance in this way is chemically incorrect as a consequence of microscopic reversibility.[13,14] Both chemical kinetics and trajectory thermodynamics show[8–12] why catalysis-driven motors must instead operate through a Brownian information ratchet mechanism.[15,16] Our group has explained and introduced[16–19] how such principles can be used in the design and construction of artificial molecular systems[16–22] and, because 'making is understanding', used them to rationalize how to give stochastic chemical processes direction.[23] Kinetic asymmetry[24–28] in the chemomechanical cycle of the machine's catalysis[3] of fuel-to-waste determines the direction of movement due to differences in reaction rate depending on the mechanical (i.e., the conformational or co-conformational) state of the system.[8]

Recently,[29] rearranging equations originally derived by Astumian allowed us to highlight parallels between kinetic asymmetry and the Curtin–Hammett principle[30,31] in catalysis-driven information ratchet mechanisms. A power stroke is simply a thermodynamic difference between (co-)conformers (energetically downhill in a positive power stoke; energetically uphill in a negative, or anti-, power stroke).[29] It can affect kinetic asymmetry as long as the introduction of the power stroke alters the transition state energies for chemical processes, so that the difference between the sum of transition states energies for the forward and backward pathway is changed.[29] Furthermore, analysis[32] based on information thermodynamics[33–35] has built on kinetic arguments[8–12] to examine the free energy transduction in a molecular motor, revealing that altering the power stroke can change the flow of free energy from a fuel-to-waste process to mechanical motion, with implications for the rate of rotation and the efficiency of a motor. This may explain why energetically substantial conformational changes are common in biomolecular machinery. The ongoing debate over the role of power strokes in the theoretical biophysics/chemistry literature, and their prevalence in biological systems,[5–7] highlights the need for experimental examples of the role of conformational changes and kinetic asymmetry in the operation of molecular information ratchets.

Molecular-level mechanistic understanding of the operation of biomolecular machines can be difficult to obtain directly due to the size and complexity of these macromolecules. A number of much smaller artificial molecular motors[18,36–45] and pumps[19,46–57] have been created, including examples of motors and pumps that operate autonomously by the same type of information ratchet mechanisms that drive biological machinery.[31,45,52,53,57] Minimalist information ratchets have harnessed free energy released through the ratchet-catalyzed decomposition of activated fluorenylmethoxycarbonyl carbonates[42,53,54] or the hydration of carbodiimides.[45,52,57] These artificial machines do not yet compete with the efficiency of their biological counterparts,[4,32,58–61] but their simplicity allows the effects of structural changes on chemically fueled dynamics to be investigated systematically.[57]

We recently described a rotaxane-based information ratchet[52] where the distribution of a macrocycle between two, effectively degenerate, fumaramide binding sites on the axle could be driven out of equilibrium by the ratchet's catalysis of a carbodiimide-to-urea fuel-to-waste reaction[3] (Figure 1A). The carbodiimide (diisopropylcarbodiimide (DIC)) reacts with the carboxylate group on the axle,

transiently forming an *O*-acyl urea barrier that prevents macrocycle shuttling between the two fumaramide groups. The *O*-acyl urea is rapidly displaced by hydroxybenzotriazole (HOBt), changing the barrier into a species that is hydrolyzed slowly on the time-scale of macrocycle shuttling kinetics. Directional bias in the macrocycle distribution on the axle is generated through kinetic asymmetry[11] in the catalyst chemical engine cycle[3] as a result of differences in the rates of reaction of the two machine co-conformers (i.e. the Curtin-Hammett principle[30,31]): The rates of both the reaction with the DIC fuel and the hydrolysis of the OBt ester barrier depend on the mechanical state (i.e., the position of the macrocycle on the axle) of the molecular machine catalyst, giving rise to double kinetic gating.[52] Varying the structure of the carbodiimide fuel and the nucleophilic catalyst allowed tuning of the kinetic asymmetry, and thus the directionality (*dist*-**n** to *prox*-**n** bias) of the ratchet catalyst, as well as the rate and efficiency of fuel use.[57]

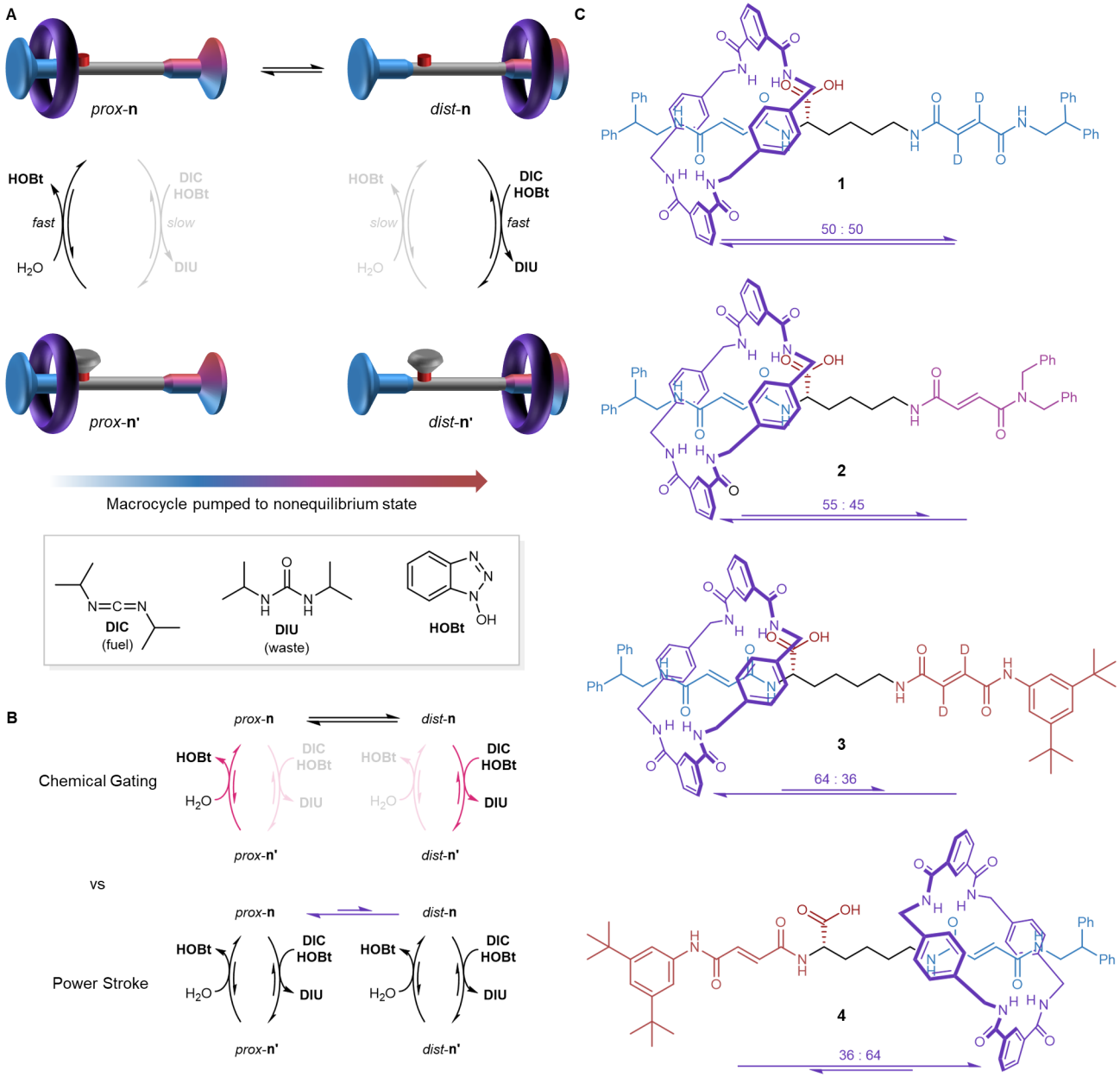

Figure 1. Design of rotaxane-based information ratchets bearing non-degenerate macrocycle binding sites on the axle.

(A) General chemomechanical cycle for the operation of the ratchets, which pump the macrocycle towards the distal binding site when fueled with a carbodiimide such as diisopropylcarbodiimide (DIC) and water in the presence of a barrier-forming nucleophilic catalyst such as hydroxybenzotriazole (HOBt) (black arrows = fast, grey arrows = slow). (B) Kinetic and thermodynamic factors can influence the machine operation. Kinetic asymmetry, arising from differences in the rate of the chemical steps dependent on the mechanical (i.e., conformational or co-conformational) state of the machine, produces directional bias in the dynamics, while a power stroke, a thermodynamic bias between (co-)conformations, can also contribute to aspects of the nonequilibrium behavior of the ratchets. (C) Structures of machines **1**–**4** with different macrocycle binding sites on the axle. Macrocycle equilibrium distributions

were determined by ^{1}H NMR spectroscopy (600 MHz, 295 K, DMSO-d_6, see Supplemental Information Section S3).

Here, we use a series of rotaxane-based molecular information ratchets with non-degenerate binding sites on the axle, to experimentally probe the roles of kinetic asymmetry and power strokes in the nonequilibrium dynamics (Figure 1). The structural modifications allow the binding energies of the fumaramide sites on the axle to be varied, providing access to rotaxanes with non-degenerate binding sites and therefore unequal distributions of rotaxane co-conformers at equilibrium. This introduces the conditions for a power stroke[5,6] in the chemomechanical cycle of the machine catalyst (Figure 1B, bottom). Comparison of the equilibrium distribution of the macrocycle on the axle with the nonequilibrium chemically-fueled steady state allows the effect of the power stroke (typically, in the examples presented, an energetically uphill, negative, power stroke) to be evaluated. We also investigate the kinetic implications of introducing non-degenerate binding sites, evaluating both the rate at which the machine reaches the chemically-fueled steady state and the catalytic efficiency of the machine for the fuel-to-waste reaction.[4] Kinetic analysis of the results provides mechanistic insight into the process and allows kinetic models to be created that predict the behavior of machines[32] that incorporate different levels of power stroke. Finally, we consider both energy and information storage in the molecular machines under nonequilibrium conditions, allowing us to make general conclusions about the design of nonequilibrium systems for specific tasks. We relate our findings to biomolecular machinery and consider the wider implications for nonequilibrium dynamic molecular systems.

RESULTS AND DISCUSSION

Synthesis of information ratchet rotaxanes with non-degenerate binding sites on the axle

Previously reported[52,57] information ratchet **1** possesses a 2,2-diphenylethylamine 'stopper' at either end of the rotaxane axle. We reasoned that structural variations in this group would change the stereoelectronic properties of the adjacent fumaramide site and, consequently, the macrocycle binding strength.[62–64] A series of rotaxanes with structural variations in either the stopper closest to the axle carboxylic acid group (proximal stopper) or the most distant one (distal stopper) were synthesized. Rotaxanes **2** and **3** feature dibenzylamine and 3,5-di-*tert*-butylaniline distal stoppers, respectively (Figure 1C). Rotaxane **4**, bearing a proximal 3,5-di-*tert*-butylaniline stopper was synthesized as an analog of rotaxane **3** with the binding site positions reversed.

Even in polar solvents, the shuttling of the macrocycle between the different fumaramide sites on the axle in ratchets **1**–**4** proved to be slow on the nuclear magnetic resonance (NMR) timescale. This allowed the equilibrium distribution of co-conformers to be determined directly by ^{1}H NMR spectroscopy (600 MHz, 295 K, DMSO-d_6, Figure 1C, see Supplemental Information, Section S3). Although significantly broadened, the ^{1}H NMR spectra of the equilibrium distribution obtained in the reaction solvent (MeCN-d_3/D_2O, 7:3 *v*/*v*) matched the ratios obtained in DMSO (Supplemental Information, Section S3). Ratchet **1**, where the proximal and distal binding sites are identical other than their distance to the carboxylic acid group, showed an even equilibrium macrocycle distribution (*prox*-**1**:*dist*-**1** = 50:50 (1:1)).[52,57] In contrast, the weaker distal binding sites in both rotaxanes **2** and **3** resulted in

uneven equilibrium macrocycle distributions which favored the proximal binding site (*prox*-**2**:*dist*-**2** = 55:45 (1.2:1), *prox*-**3**:*dist*-**3** = 64:36 (1.8:1), Figure 1C, 2). As fueling should result in the macrocycle being pumped towards the distal binding site of these ratchets, the favoring of the proximal binding site at equilibrium in this series of ratchets can be considered a negative power stroke, that is the thermodynamic bias for movement is opposite to the kinetic driving force of the information ratchet mechanism. Rotaxane **4** displayed the opposite equilibrium distribution to rotaxane **3** (*prox*-**4**:*dist*-**4** = 36:64 (1:1.8), Figure 1C, 2), constituting a positive power stroke. Unfortunately, however, poor solubility of **4** under the required reaction conditions prevented its investigation under chemical fueling.

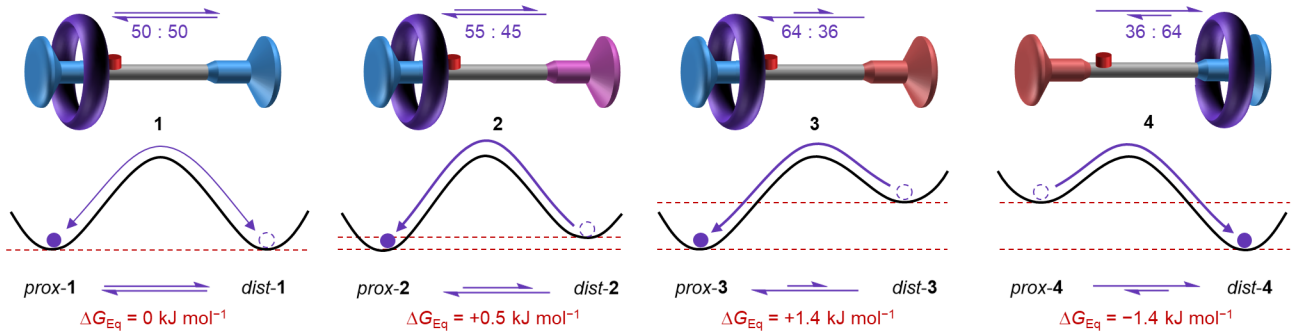

Figure 2. Different macrocycle distributions at dynamic equilibrium in rotaxane-based ratchets 1–4.

The different distributions of the macrocycle on the axle in ratchets **1**–**4** are caused by differences in the binding free energy between the non-degenerate binding sites on the axle. The free energy difference, which is formally a power stroke, is calculated from the equilibrium constant.

Autonomous chemically fueled operation of molecular ratchets 1–3

Ratchets **1**–**3** were each fueled under identical[52,57] buffered conditions using DIC as a carbodiimide fuel[4,65–69] and HOBt as a transient barrier-forming nucleophile ([ratchet] = 2.5 mM, [HOBt] = 5.0 mM, [DIC] = 12.5 mM, in 2-(*N*-morpholino)ethanesulfonic acid (MES)-buffered (100 mM, pH_{obs} 5.36) MeCN-d_3/D_2O (7:3 *v*/*v*), see Supplemental Information, Section S4.1 and S5.1). Addition of *para*-methoxybenzylamine at different timepoints of the fueled reaction irreversibly formed a stable amide, kinetically trapping the nonequilibrium macrocycle distribution at that timepoint,[52,57,70] which could be subsequently analyzed by ^{1}H NMR spectroscopy (see Supplemental Information, Section S4.1).

Over the course of fueled operation, the ratio of *prox*-**n′** :*dist*-**n′** decreased for all three ratchets, following a pseudo-first order rate profile (see Supplemental Information, Figure S5 for kinetic fitting). The three ratchets reached different steady state ratios with the time taken to reach the steady state also varying for the different ratchets (Figure 3A). Ratchet **1** reached a steady state ratio of 1:20, *prox*-**1′** :*dist*-**1′** after 17.4 h, ratchet **2** reached a steady state ratio of 1:17, *prox*-**2′** :*dist*-**2′** after 13.4 h and ratchet **3** reached a steady state ratio of 1:12, *prox*-**3′** :*dist*-**3′** after 10.2 h (Table 1).

Kinetic analysis of nonequilibrium behavior of chemically-fueled molecular ratchets 1–3

Ratchets **1**–**3** pump to different steady state ratios, with the most negative power stroke, ratchet **3**, resulting in the lowest steady state ratio of 8:92 (1:12), *prox*-**3′** :*dist*-**3′** at the steady state. Superficially, it may appear that this ratchet is therefore closer to equilibrium and is consequently doing less work to maintain the nonequilibrium steady state. However, this is incorrect as the equilibrium distribution of ratchet **3** (64:36 (1.8:1), *prox*-$\mathbf{3}_{Eq}$:*dist*-$\mathbf{3}_{Eq}$) favors the proximal binding site. Indeed, the observed steady state macrocycle distribution ratios correlate almost perfectly ($R^2 > 0.99$) with the different equilibrium macrocycle distribution ratios (Figure 3B). This is because, as predicted by kinetic analysis,[8–12] kinetic asymmetry is solely responsible for determining the directionality of the molecular ratchet, and changing a binding site does not necessarily result in a change in kinetic asymmetry. Kinetic asymmetry acts as a modifier to what the distribution was at equilibrium, increasing the distal to proximal ratio by the same proportion regardless of the ratio at equilibrium (see equation, Figure 3B). Consequently, the gradient of the correlation in Figure 3B is equal to the kinetic asymmetry of the ratchet under the experimental conditions used for the chemical fueling, quantified by the ratcheting constant, K_r = 20.6 (see Supplemental Information, Section S4.2). The data can be normalized to reflect the constant kinetic asymmetry of the ratchet (Figure 3C), resulting in directionality profiles that converge on the same steady state within error (see Supplemental Information, Section S4.3 for full details of the normalization of directionality).

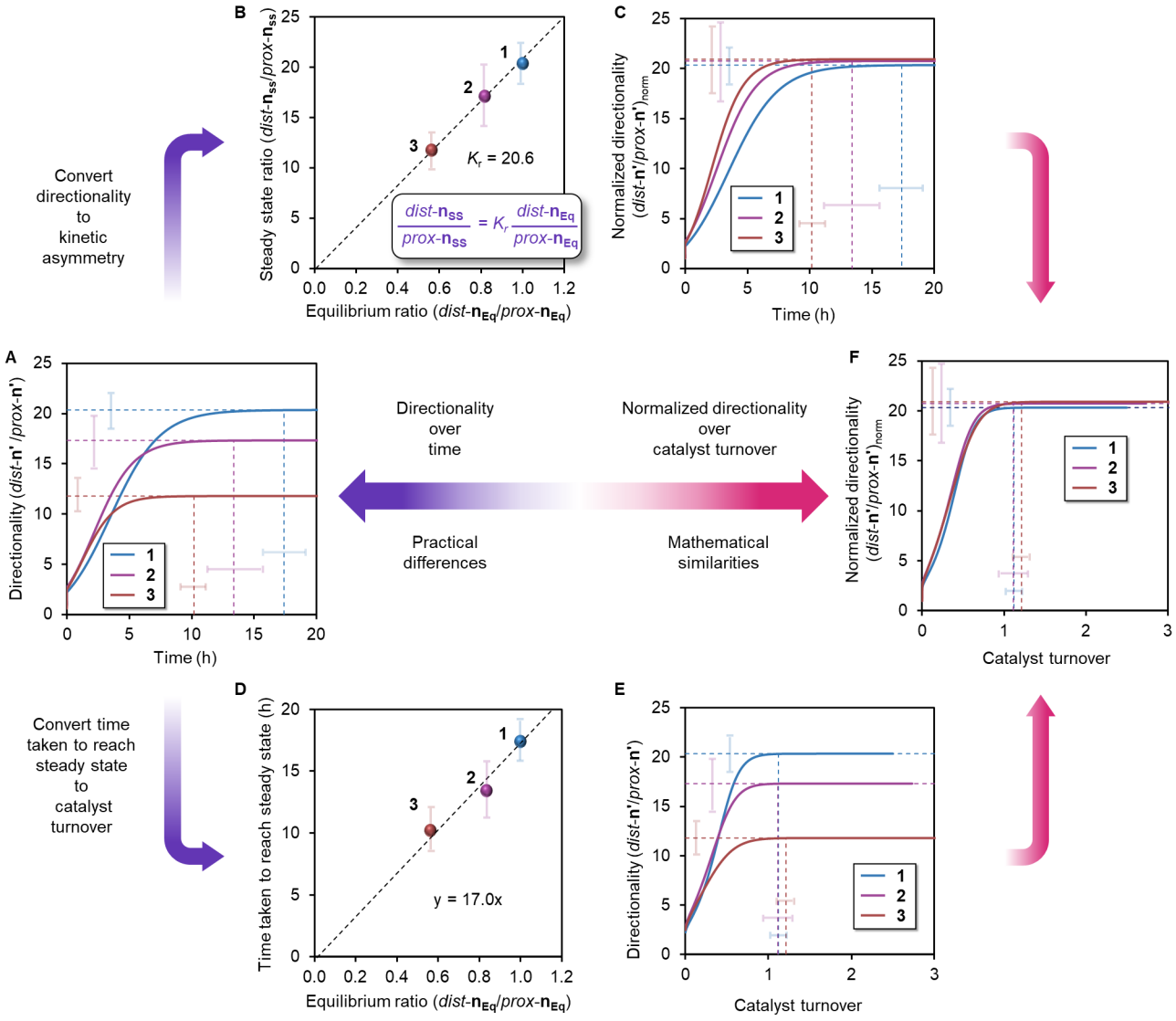

Figure 3. Nonequilibrium behavior of chemically fueled rotaxane information ratchets 1–3.

(A) The bias in the macrocycle distribution introduced by ratchets **1**–**3** upon fueling with DIC was analyzed by kinetic trapping through addition of *p*-methoxybenzylamine to aliquots taken at various time intervals (see Supplemental Information, Section S4.1). The *dist*-**n′** /*prox*-**n′** ratio increases during fueling until it reaches a steady state. Ratchets **1**–**3** show approximately the same initial ratio (*dist*-**n′** /*prox*-**n′** ≈ 2.4), but the more proximal favoring ratchets reach lower steady state ratios, albeit more quickly than less proximal favoring ratchets. (B) The steady state ratios correlate well ($R^2 > 0.99$) with the equilibrium ratios, demonstrating that the kinetic asymmetry, given by the gradient ($K_r = 20.6$), is the same for all three ratchets, **1**–**3**. (C) Normalized directionality curves show approximately the same initial and steady state biases, although ratchets **2** and **3** reach the chemically fueled steady state more rapidly than ratchet **1**. (D) The time taken to reach the chemically fueled steady state correlates well with the equilibrium ratio ($R^2 > 0.99$), suggesting a causal link to the power stroke. (E) When the catalytic turnover (the average number of fuel-

to-waste cycles performed by the ratchet, see Supplemental Information, Section S4.5) is accounted for, ratchets **1**–**3** reach their chemically fueled steady states after the same number of fuel-to-waste cycles. (F) Combining the normalized directionality shown in panel C with the catalyst turnover shown in panel E, the curves for all three ratchets overlap. Errors are determined based on the standard deviation of the fit of the experimental data to a first order rate equation and standard error propagation (see Supplemental Information, Section S6 for full details of error treatment).

Perhaps less intuitively, the time taken for each ratchet to reach steady state also correlates with the equilibrium macrocycle distribution (Figure 3D) ($R^2 > 0.99$). Ratchet **3**, with the most negative power stroke, reaches the chemically fueled steady state after only 10.2 hours under the operating conditions, about 1.7× faster than ratchet **1**. Although the time taken to reach the steady state is different for each ratchet, each ratchet also catalyzes the fuel-to-waste reaction at different rates (see Supplemental Information, Section S5). However, if the catalyst turnover of each ratchet is taken into account, the result is rate profiles in which the chemically fueled steady state is reached after the same catalyst turnover (~1.2 completed cycles on average, see Supplemental Information, Section S4.5) for each ratchet (Figure 3E). Combining the treatment of the data to plot normalized directionality against catalyst turnover results in overlapping rate profiles for each ratchet (Figure 3F).

Table 1. Parameters describing the operation of ratchets 1-3

See Supplemental Information, Section S4 for full derivation of parameters. Errors are determined based on the standard deviation of the fit of the experimental data to a first order rate equation and standard error propagation.

Ratchet	Equilibrium ratio (*dist*-**n**/*prox*-**n**)[a]	Initial trapped ratio (*dist*-**n′** /*prox*-**n′**)[b]	Steady state ratio (*dist*-**n′** /*prox*-**n′**)[b]	Chemical gating of ester formation[c]	Chemical gating of ester hydrolysis[d]	Ratcheting constant,[e] K_r	Time to reach steady state[b] / h	Rate of catalyzed reaction[f] / $\times 10^{-6}$ s^{-1}
1	1.00 ± 0.05	2.2 ± 0.2[g]	20 ± 2	2.2 ± 0.1	9.3 ± 0.9	20 ± 2	17.4 ± 1.7	8.5 ± 0.1
2	0.83 ± 0.05	2.7 ± 0.3[g]	17 ± 3	3.2 ± 0.2	6.5 ± 1.4	21 ± 4	13.4 ± 2.3	13.9 ± 0.1
3	0.56 ± 0.04	2.4 ± 0.2[g]	12 ± 1	4.3 ± 0.3	4.8 ± 0.8	21 ± 4	10.2 ± 1.1	14.8 ± 0.1

[a] Determined by ^{1}H NMR spectroscopy (600 MHz, 295 K, DMSO-d_6) of ratchets at equilibrium.
[b] Determined by ^{1}H NMR spectroscopy (600 MHz, 295 K, DMSO-d_6) of *para*-methoxybenzylamide adducts of ratchets in fueling experiments (see Figure 3A).
[c] Calculated from equilibrium ratio (power stroke) and initial trapped ratio.
[d] Calculated from initial trapped ratio and the steady state ratio.
[e] Calculated from the equilibrium ratio (power stroke) and steady state ratio.
[f] Determined from rate of fuel use in presence of the ratchet minus the rate background fuel use.
[g] Errors based on ^{1}H NMR integrals. Other sources of error, such as ratchets undergoing multiple cycles prior to amide formation or inherent reactivity differences as a result of structural differences, are not accounted for.

The nonequilibrium kinetics provide insight into the mechanism of operation of ratchets **1**–**3**. The best agreement with kinetic models is observed when the differences in transition state energies for both ester formation and hydrolysis remain constant,[8–12] that is $\Delta G_{TS}^{\ddagger}$ ester formation and $\Delta G_{TS}^{\ddagger}$ ester hydrolysis are unchanged across all three ratchets (Figure 4, pink, see Supplemental Information, Section S7). The unchanging transition state energy difference implies that the macrocycle is involved in stabilizing the transition state for both distal ester formation ([*dist*-$\mathbf{n}^{Est}$]‡) and hydrolysis ([*dist*-$\mathbf{n}^{Hyd}$]‡). Considered in terms of the Curtin-Hammett principle,[29] the population bias introduced by the power stroke (K_{Eq}, *dist*-$\mathbf{n}_{Eq}$/*prox*-$\mathbf{n}_{Eq}$) is perfectly balanced by the corresponding change in the chemical gating of the steps (ratio of

rates, k_{dist}/k_{prox}). This effect accounts for a number of observations. The initial ratio of *prox*-**n'**:*dist*-**n'** (obtained by trapping at 0 h, Figure 3A) is the same for all three ratchets (*dist*-**n'**/*prox*-**n'** ≈ 2.4, see Table 1). This shows that the difference between the transition state energies for proximal and distal ester formation ([*prox*-$\mathbf{n}^{Est}$]‡ and [*dist*-$\mathbf{n}^{Est}$]‡ respectively, Figure 4A, pink) is unchanged across the ratchets, as this is the sole feature that determines the initial *prox*-**n'**:*dist*-**n'** ratio.[29] In practical terms, introducing a power stroke in this manner biases the equilibrium population of *prox*-**n**:*dist*-**n** but also increases the rate of the *dist*-**n**→*dist*-**n'** reaction proportionally, increasing the chemical gating by the same factor as the power stroke (Table 1). However, the steady state ratios are different across ratchets **1**–**3**, requiring that the chemical gating of the ester hydrolysis step is different across the three ratchets (Table 1, Figure 3A). The ester hydrolysis is a kinetic (rather than a dynamic kinetic) resolution (Figure 4B), thus the activation energy for *dist*-$\mathbf{n}^{OBt}$→[*dist*-$\mathbf{n}^{Hyd}$]‡ varies between ratchets **1**–**3**. The increase in the chemical gating of the ester formation as a consequence of a more negative power stroke being introduced (Table 1), is negated by a corresponding decrease in the chemical gating of the ester hydrolysis, resulting in a value of kinetic asymmetry that is consistent across all three ratchets. Moreover, the data indicate that the equilibrium distribution between the carboxylate and -OBt ester forms of rotaxanes **1**–**3** remains unchanged (see Supplemental Information, Section S7).

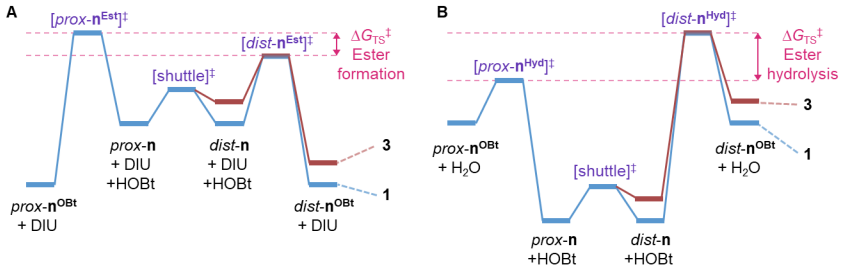

Figure 4. Illustrative reaction profiles for rotaxane information ratchets 1–3

Reaction profile (not to scale) for (A) ester formation and (B) ester hydrolysis for ratchet **1** (degenerate binding sites, blue), and ratchet **3** (distal site macrocycle binding affinity is weaker, changes shown in red). The experimental kinetic data indicates that the difference in transition state energies ($\Delta G_{TS}^{‡}$, pink) remains unchanged between ratchets **1**–**3**, regardless of changes in the distal binding site affinity. Note that panel A corresponds to a Curtin-Hammett diagram for a dynamic kinetic resolution during ester formation, while panel B depicts a non-dynamic kinetic resolution for ester hydrolysis, where the products of the reaction, rather than starting materials, exchange.

Another feature of the mechanism that is apparent from the experimental data analysis is that the catalytic efficiency[4] of ratchets **1**–**3** varies, resulting in faster catalysis for ratchets with a more negative power stroke. This effect is largely a manifestation of the lower activation energy of the distal ester hydrolysis (*dist*-$\mathbf{n}^{OBt}$→[*dist*-$\mathbf{n}^{Hyd}$]‡), as well as the greater population of *prox*-$\mathbf{n}^{OBt}$ for the more biased ratchets (Table 1, Figure 4B), both of which accelerate the rate-limiting hydrolysis step in the catalytic cycle. This greater rate of fuel consumption also explains why the more biased ratchets reach the chemically fueled steady state faster (Figure 3D), given that the ratchets use the same amount of fuel (within error) to reach the same normalized directionality (Figure 3F).

There are practical consequences arising from the presence and magnitude of power strokes that could have implications for certain applications. A positive power stroke (such as in ratchet **4**) combines the thermodynamic bias with the kinetic driving force, and may therefore reach a greater absolute directionality at the chemically fueled steady state, which might be beneficial in certain circumstances.[9,32,71] By contrast, ratchets employed in signaling applications[72–75] may benefit from a negative power stroke (such as in ratchets **2** and **3**), as it may enable them to reach a chemically fueled steady state faster and therefore transmit signals more frequently.

The data obtained with rotaxanes **1**–**3** also informs the expected behavior of other types of related information ratchet motors. Joining the ends of rotaxane **3** and adding a second carboxylate catalytic site would create a catenane-based rotary motor analogous to the system previously reported by Wilson et al.[42] (see Supplemental Information, Section S8). Such a catenane motor, with non-degenerate component binding sites, would pay penalties for both the lower directionality arising from the thermodynamically uphill step and for the slower reaction rate caused by the downhill step, resulting in a poorer motor with lower thermodynamic efficiency.[4] This is consistent with the information thermodynamic analysis of similar motors that predicted[32] that, irrespective of the importance of kinetic asymmetry,[8–12] the maximum thermodynamic efficiency is reached when the binding sites are degenerate (i.e. the minima along the reaction pathway are as similar in energy as possible). This illustrates well that although the kinetics of non-equilibrium molecular machines are crucial to their operation, further insights follow from considering the free energy flow in such systems.[2,32,76]

Information thermodynamics analysis of nonequilibrium behavior

We also used the experimental kinetic data to inform a thermodynamic model of the nonequilibrium behavior of molecular ratchets.[32] It has previously been demonstrated that the ratcheting constant (K_r) sets an upper limit on the amount of free energy that can be 'stored' in a nonequilibrium system.[77,78] However, such a limit can only be reached when the fueling cycle is infinitely fast. The experimental data obtained upon chemically fueling **1**–**3** enables the free energy that can be stored within an information ratchet to be studied in terms of the observed directionality at steady state.[79]

We applied tools from nonequilibrium thermodynamics of open chemical reaction networks[80,81] to quantitatively access the energetics of rotaxane information ratchets **1**–**3**, dissecting contributions to the free energy stored in each ratchet into an information (Shannon entropy[33,82]) component and a binding free energy (that is given by the standard chemical potential difference between the two co-conformers multiplied by the proportion of macrocycles shifted with respect to equilibrium) component (Figure 5).[35,83,84] In particular, we focused on the shuttling of the macrocycle and determined how free energy is stored in the mechanical degree of freedom (see Supplemental Information, Section S9.1 for details and validation of this coarse-graining). The chemically fueled nonequilibrium operation of the ratchets can be regarded simply as shifting the distribution of the macrocycle on the axle, allowing changes in binding free energy, information, and total free energy to be calculated (equation 1, Figure 5A).

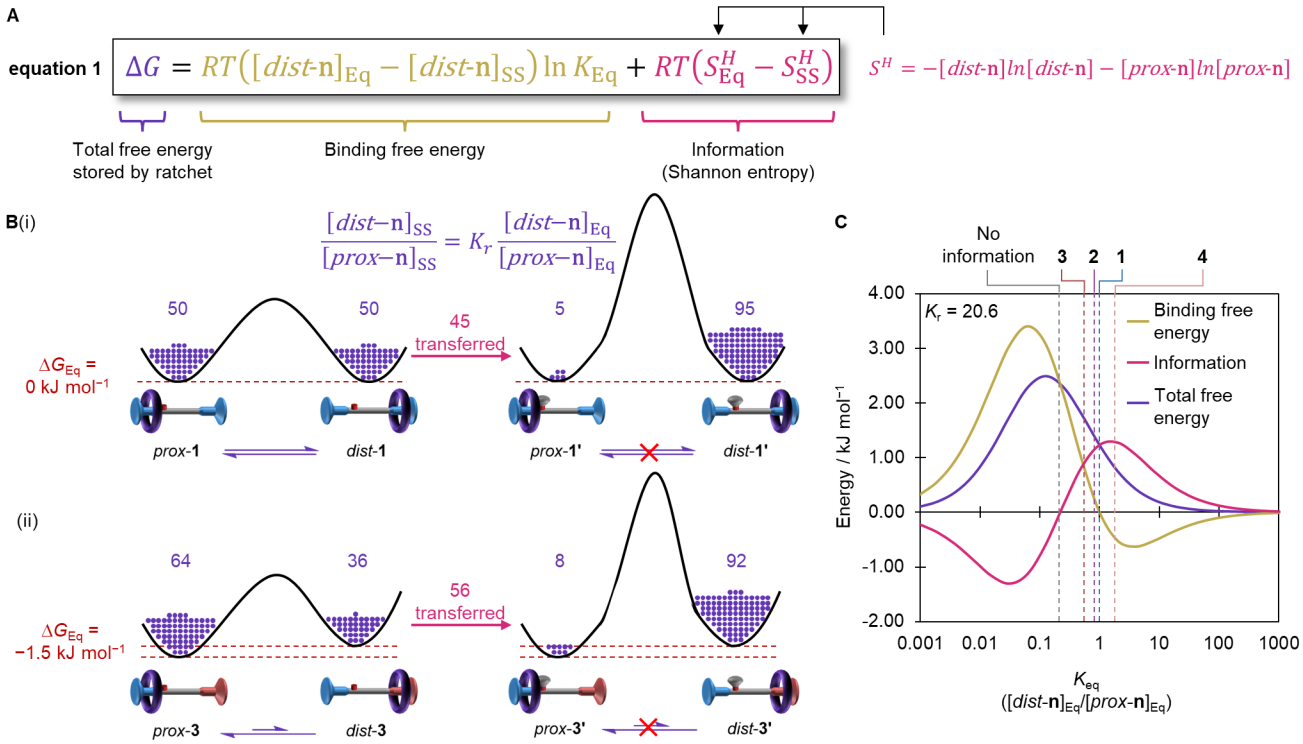

Figure 5. Nonequilibrium thermodynamics of rotaxane information ratchets 1–3

(A) Equation 1 describes the total free energy (ΔG) stored by the ratchets at the chemically fueled steady state and is composed of two components: the binding free energy (yellow) and the information or Shannon entropy (pink). The former component (yellow) comprises the difference between [*dist*-**n**] at the chemically fueled steady state (subscript SS) and at equilibrium (subscript Eq), multiplied by the power stroke, given by the natural logarithm of the equilibrium constant (K_{Eq}) for *dist*-$\mathbf{n}_{Eq}$/*prox*-$\mathbf{n}_{Eq}$. The latter component (pink) in the equation is the difference between the Shannon entropy (S^H) at equilibrium and the chemically fueled steady state. In both parts of the equation, R is the gas constant and T is the temperature in Kelvin. Therefore, Equation 1 is expressed in units of energy per volume, which can be converted in units of energy per mole (used in the main text) by dividing by the total concentration of ratchet. (B) The proportion of macrocycles that must move *prox*→*dist* to reach the chemically fueled steady state and satisfy K_r differs between the ratchets. (i) a net 45% of macrocycles must be transported *prox*→*dist* for ratchet **1**, (ii) whereas a net 56% of macrocycles must move to increase the ratio by the same proportion (K_r) in ratchet **3**. (C) The dependencies of the binding free energy (yellow), information (pink) and total free energy (purple) on K_{Eq}, have several distinct domains (see Table 2). K_r is assumed to also be 20.6 for ratchet **4**.

Table 2. Calculated thermodynamic parameters describing the operation of ratchets 1–4 and theoretical ratchets with K_r = 20.6

Listed in order of decreasing K_{Eq} (as shown by the equilibrium ratio). See Supplemental Information, Section S9 for full derivation of parameters based on equation 1, Figure 5.

Ratchet	Equilibrium ratio *prox*-**n**:*dist*-**n**	Steady state ratio *prox*-**n′**:*dist*-**n′**	Binding energy difference between stations / kJ mol^{-1}	Macrocycles moved / %	Total free energy stored / kJ mol^{-1}	Information (Shannon entropy) stored / kJ mol^{-1}	Binding free energy stored / kJ mol^{-1}
4[a]	36:64	3:97	−1.41	33	0.83	1.29	−0.47
Maximum information	39:61	3:97	−1.05	36	0.92	1.30	−0.38
1[a] (No binding free energy)	50:50	5:95	0.00	45	1.23	1.23	0.00
2[a]	55:45	6:94	0.45	49	1.38	1.16	0.22
3[a]	64:36	8:92	1.41	56	1.71	0.91	0.79
No information	82:18[b]	18:82	3.69	64	2.36	0.00	2.36
Maximum total free energy	89:11	28:72	5.07	61	2.49	−0.59	3.09

[a] Equilibrium position determined by integration of slowly interconverting co-conformers in DMSO-d_6 at 295 K using ^{1}H NMR spectroscopy.
[b] Calculated as $(K_r)^{-1/2}$

Rotaxane **1**, bearing degenerate macrocycle binding sites on the axle, is a direct molecular analogue of a single-particle Maxwell's Demon or Szilard Engine thought experiment.[16,19,33,85,86] In rotaxane **1** the free energy arising from a non-equilibrium distribution of the macrocycle on the axle can only be stored as information since the intercomponent binding free energy is the same whether the macrocycle is on the distal or proximal fumaramide site. As illustrated in Figure 5B, the distribution of the macrocycle between proximal and distal sites is 50:50 at equilibrium, a condition that maximizes Shannon entropy and gives no prior information about the location of the macrocycle (the location can be guessed with a 50% certainty). This binary system is analogous to an unbiased coin toss and related to one bit of information in computer memory; there is a well-defined maximum of information that can be stored (one bit = k_BT ln(2) corresponding to 1.69 kJ mol^{-1} at 20 °C).[33] Upon fueling, rotaxane **1** reaches a nonequilibrium steady state with a 5:95 *prox*-**1′**:*dist*-**1′** distribution, corresponding to movement of 45% of the macrocycles from the proximal to the distal binding site (50:50→5:95, Figure 5B). Consequently, at the chemically fueled steady state the location of the macrocycle is known with a 95% certainty. The increase in information about the macrocycle position upon going from the equilibrium to the nonequilibrium steady state can be quantified by the decrease in the Shannon entropy value, which, in this case, is proportional to the free energy stored by the system at the steady state (calculated as 1.23 kJ mol^{-1}, Table 2) since there is no difference in binding free energy between the two axle binding sites.

Changing the macrocycle binding sites of the ratchets alters the form in which free energy is stored at the steady state. For instance, rotaxane **3** goes from a 64:36 *prox*-**3**:*dist*-**3** ratio at equilibrium to 8:92 at the chemically fueled steady state, corresponding to the transfer of 56% of the macrocycles from the proximal to the distal binding site (Figure 5B). Shannon entropy is reduced, thus storing information (calculated at 0.91 kJ mol^{-1}, Table 2). However, since at equilibrium rotaxane **3** already stores some information, the maximum amount of free energy that can be

stored as Shannon entropy is inherently reduced. Instead, when the distal binding site is made less favorable at equilibrium, such as for rotaxanes **2** and **3**, some energy must be spent breaking the stronger interactions at the proximal site to pump the ring towards the distal site. The binding free energy stored at the steady state corresponds to the binding site free energy difference (determined from the equilibrium distribution, Figure 2) multiplied by the proportion of macrocycles moved (which is dictated by the ratcheting constant). For example, the binding site free energy difference for ratchet **3** is 1.4 kJ mol^{-1}, resulting in 0.56 × 1.4 kJ mol^{-1} = 0.79 kJ mol^{-1} stored as binding free energy. Rotaxane **3** therefore stores less information at the chemically fueled steady state than rotaxane **1**, but due to the binding free energy contribution, overall, **3** stores more free energy than **1** (total free energy = binding free energy + Shannon entropy = 0.79 kJ mol^{-1} + 0.91 kJ mol^{-1} = 1.71 kJ mol^{-1}) and can therefore be considered 'further from equilibrium' from a thermodynamic viewpoint.

We simulated the change in binding free energy, information and total free energy of ratchets **1**–**3** as a function of the equilibrium macrocycle distribution at a constant kinetic asymmetry, K_r of 20.6, reflecting the experimental data under chemical fueling (Figure 5C, see Supplemental Information, Section S9.3 for the effect of varying K_r). The simulation illustrates how introducing a power stroke changes the energetics of the information ratchet. When a sufficiently large binding free energy difference between the two axle binding sites is introduced (extreme left or right of Figure 5C), the ratchet stalls: the equilibrium distribution is so biased towards one site that shifting it by a factor of K_r does not result in an appreciable change in the thermodynamic quantities. However, at intermediate binding free energy differences (~99:1–1:99 *prox*-$\mathbf{n_{Eq}}$:*dist*-$\mathbf{n_{Eq}}$), the form in which free energy is stored at the steady state can change dramatically. Free energy can be stored solely as information (blue dashed line, corresponding to the degenerate rotaxane **1**) or solely as binding free energy (gray dashed line). In the latter case, the equilibrium and steady state distributions are exact opposites, so the total amount of information in the system is unchanged moving from equilibrium to the chemically fueled steady state (82:18→18:82). To the left of this point, the steady state distribution is less-biased than the equilibrium distribution, so information is erased upon moving from equilibrium to the chemically fueled steady state (Shannon entropy is increased), while to the right, moving from equilibrium to the chemically fueled steady state increases information (Shannon entropy is decreased). We note that the information component is anti-symmetric, as it relates to the macrocycle distribution over the two binding sites at equilibrium and steady state, while the binding free energy component shows an asymmetric profile, as it relates to the net number of macrocycles pumped from the proximal site to the distal site (see Supplemental Information, Section S9.3).

The simulation also identifies equilibrium ratios at which the binding free energy, information and total free energy storage can be maximized (Figure 5C, maxima of yellow, pink and purple lines respectively). Based on its observed equilibrium ratio (36:64 *prox*-$\mathbf{4_{Eq}}$:*dist*-$\mathbf{4_{Eq}}$), rotaxane **4** is predicted to be well-optimized for maximizing information storage (when K_r = 20.6). The maximum binding free energy (Figure 5C, yellow) corresponds to the point at which the proportion of net-displaced macrocycles multiplied by the energy difference reaches a maximum. Consequently, as K_r is increased, this point will move further left on the graph (towards a more negative power stroke), accompanied by an increase in the maximum free energy.

Information storage for this type of rotaxane ratchet with a K_r = 20.6 reaches a maximum with a modest positive power stroke, close to the actual distribution found in rotaxane **4**, balancing the bias introduced when moving from equilibrium to the chemically fueled steady state against the number of net-displaced macrocycles. The position of the maximum tends towards a 50:50 equilibrium distribution (K_{Eq} = 1) as the ratcheting constant is increased. The total free energy stored is the sum of the binding free energy and information (equation 1, Figure 5A), and at its maximum is dominated by the binding free energy (particularly for large values of K_r), which is not inherently limited in the same way as information is in a binary system. However, in a similar manner to the way that information storage is limited to one bit in a binary system,[28] the equilibrium difference in binding free energy defines the maximum free energy that can be stored in this form as K_r tends towards infinity.

The experimental data obtained from chemically fueling rotaxanes **1**–**3** highlight the importance of taking into account the power stroke when considering the nonequilibrium function of the ratchet. Appropriate selection of the size and sign of a power stroke can significantly increase the free energy a ratchet can store.[87,88] Under the experimental conditions of chemical fueling with K_r = 20.6, ratchet **3** stored 1.4x more free energy than ratchet **1**, while the maximum possible free energy stored is more than double that stored by ratchet **1** (Table 2, maximum total free energy)! If, instead, the ratchet is intended to store (or process) information,[89–93] the optimal distribution would be to favor the distal site slightly and therefore have a negative binding free energy contribution. These observations have implications for the design of ratchets for functions in molecular computing[74,83] and sensing,[75,76,89,90] compared to ratchets that drive motors, perform work against a force, or are required to maintain a high energy state.[87,88]

Conclusions

In summary, the roles of kinetic asymmetry and power strokes have been determined in a series of rotaxane-based information ratchets that have different macrocycle binding affinities at two axle sites. It was experimentally demonstrated that kinetic asymmetry was not influenced by the introduction of such a power stroke. The changes between the dynamic equilibrium and chemically fueled steady state distributions of the macrocycle on the axle in the rotaxane series correlate ($R^2 > 0.99$), with a gradient corresponding to the kinetic asymmetry of the chemically fueled information ratchet, K_r, of 20.6. Moreover, the ratchets all catalyze the same amount of fuel-to-waste to reach their chemically fueled steady state regardless of the negative power stroke that has to be overcome. However, the presence of the power stroke does have consequences: The chemically fueled steady state macrocycle distribution is determined by a combination of the power stroke and the chemical gating, and the time taken to reach the steady state is reduced with an increasingly negative power stroke. This may be useful to take into account when designing chemically fueled ratchets for specific applications where the speed of ratcheting or the degree of positional bias of the components is important.

The presence of a power stroke also has a profound influence on the free energy stored by the ratchet, affecting both the total free energy stored and the relative contributions to this stored energy of information (Shannon entropy) and inter-component binding free energy. Simulations show how this partitioning of the free energy varies as a function of the power stroke, thus enabling the identification of optimal power strokes for specific purposes, for example for maximizing free energy storage or maximizing information storage. Such considerations may be particularly

helpful when designing ratchets for applications involving information processing. The influence of power strokes on these different types of features may explain why they are so prevalent in biomolecular machinery, where evolution has optimized different features of the mechanism for particular functions.[2,94–97]

Since 'making is understanding',[23] the structure-property relationships obtained using these minimalist artificial ratchets reveal tangible concepts for how performance can be optimized in nonequilibrium systems. The results provide experimental data that can be used to both inform and to test theoretical models.[98] These are amongst the first experimental systems that are structurally and dynamically simple enough to demonstrate and quantify the interaction between enthalpy and entropy in a nonequilibrium regime. Exploring such relatively minimalistic chemically fueled molecular devices furthers the understanding of nonequilibrium behavior on the nanoscale. This may aid the answering of profound fundamental questions relating to the out-of-equilibrium behavior of chemically fueled biological systems and, ultimately, how chemistry becomes biology.

EXPERIMENTAL PROCEDURES

Resource availability

Lead contact

Further information and requests for resources should be directed to and will be fulfilled by the lead contact, David A. Leigh (david.leigh@manchester.ac.uk).

Materials availability

This study did not generate new materials.

Data and code availability

The datasets generated during this study are included in the supplemental information. Simulation files of the nonequilibrium free energy dependencies of the ratchets where the inputs may be altered are available as an Excel file and a Jupyter notebook as part of the Supplemental Information.

SUPPLEMENTAL INFORMATION

Document S1. Supplemental experimental procedures and further discussion, Schemes S1–S5, Figures S1–S18, Tables S1–S16, and Spectra S1–S40.

Document S2. Nonequilibrium free energy dependancies.xlsx

ACKNOWLEDGMENTS

We acknowledge support from the European Research Council (ERC Advanced Grant 786630), the Engineering and Physical Sciences Research Council (EPSRC) (Grant EP/P027067/1), the Gordon and Betty Moore Foundation (Grant GBMF10790 to T.R.G.), and the University of Manchester and EPSRC for Ph.D. studentships to L.B. and B.M.W.R. D.A.L. is a Royal Society Research Professor.

AUTHOR CONTRIBUTIONS

S.B. and B.M.W.R. devised the project. L.B. carried out the synthesis and kinetics experiments, aided by S.B. and B.M.W.R. L.B., B.M.W.R. and E.P. conducted the kinetic analysis. E.P., B.M.W.R. and T.R.G. conducted the thermodynamic analysis.

S.B. and D.A.L. directed the research. All authors contributed to the writing of the manuscript.

DECLARATION OF INTERESTS

The authors declare no competing interests.

REFERENCES

1. Schliwa, M., and Woehlke, G. (2003). Molecular motors. Nature *422*, 759–765. 10.1038/nature01601.
2. Brown, A. I., and Sivak, D. (2020). Theory of nonequilibrium free energy transduction by molecular machines. Chem. Rev. *120*, 434–459. 10.1021/acs.chemrev.9b00254.
3. Amano, S., Borsley, S., Leigh, D. A., and Sun, Z. (2021). Chemical engines: driving systems away from equilibrium through catalyst reaction cycles. Nat. Nanotechnol. *16*, 1057–1067. 10.1038/s41565-021-00975-4.
4. Borsley, S., Leigh, D. A., and Roberts, B. M. W. (2022) Chemical fuels for molecular machinery. Nat. Chem. *14*, 728−738. 10.1038/s41557-022-00970-9.
5. Wagoner, J. A., and Dill, K. A. (2016). Molecular motors: power strokes outperform Brownian ratchets. J. Phys. Chem. B *120*, 6327–6336. 10.1021/acs.jpcb.6b02776.
6. Hwang, W., and Karplus, M. (2019). Structural basis for power stroke vs. Brownian ratchet mechanisms of motor proteins. Proc. Natl. Acad. Sci. U. S. A. *116*, 19777–19785. 10.1073/pnas.1818589116.
7. Howard, J. (2006). Protein power strokes. Curr. Biol. 2006, *16*, R517–R519. 10.1016/j.cub.2006.06.045.
8. Astumian, R. D. (2015). Irrelevance of the power stroke for the directionality, stopping force, and optimal efficiency of chemically driven molecular machines. Biophys. J. *108*, 291−303. 10.1016/j.bpj.2014.11.3459.
9. Astumian, R. D., Mukherjee, S., and Warshel, A. (2016). The physics and physical chemistry of molecular machines. ChemPhysChem *17*, 1719−1741. 10.1002/cphc.201600184.
10. Astumian, R. D. (2017). How molecular motors work - insights from the molecular machinist's toolbox: the Nobel prize in Chemistry 2016. Chem. Sci. *8*, 840−845. 10.1039/C6SC04806D.
11. Astumian, R. D. (2019). Kinetic asymmetry allows macromolecular catalysts to drive an information ratchet. Nat. Commun. *10*, 3837. 10.1038/s41467-019-11402-7.
12. Astumian, R. D., Pezzato, C., Feng, Y., Qiu, Y., McGonigal, P. R., Cheng, C., and Stoddart, J. F. (2020). Non-equilibrium kinetics and trajectory thermodynamics of synthetic molecular pumps. Mater. Chem. Front. *4*, 1304−1314. 10.1039/D0QM00022A.
13. Lewis, G. N. (1925). A new principle of equilibrium. Proc. Natl. Acad. Sci. U. S. A. *11*, 179–183. 10.1073/pnas.11.3.179.
14. Tolman, R. C. (1925). The principle of microscopic reversibility. Proc. Natl. Acad. Sci. U. S. A. *11*, 436–439. 10.1073/pnas.11.7.436.
15. Bier, M. (1997). Brownian ratchets in physics and biology. Contemp. Phys. *38*, 371–379. 10.1080/001075197182180.
16. Kay, E. R., Leigh, D. A., and Zerbetto, F. (2007). Synthetic molecular motors and mechanical machines. Angew. Chem. Int. Ed. *46*, 72−191. 10.1002/anie.200504313.
17. Zhang, L., Marcos, V., and Leigh, D. A. (2018). Molecular machines with bio-inspired mechanisms. Proc. Natl. Acad. Sci. USA 115, 9397−9404. 10.1073/pnas.1712788115.
18. Hernández, J. V., Kay, E. R., and Leigh, D. A. (2004). A reversible synthetic rotary molecular motor. Science *306*, 1532–1537. 10.1126/science.1103949.
19. Serreli, V., Lee, C.-F., Kay, E. R., and Leigh, D. A. (2007). A molecular information ratchet. Nature *445*, 523–527. 10.1038/nature05452.
20. Heard, A. W., and Goldup, S. M. (2020). Simplicity in the design, operation, and applications of mechanically interlocked molecular machines. ACS Cent. Sci. *6*, 117−128. 10.1021/acscentsci.9b01185.
21. Aprahamian, I. (2020). The future of molecular machines. ACS Cent. Sci. *6*, 347–358. 10.1021/acscentsci.0c00064.
22. Feng, Y., Ovalle, M., Seale, J. S. W., Lee, C. K., Kim, D. J, Astumian, R. D., and Stoddart, J. F. (2021). Molecular pumps and motors. J. Am. Chem. Soc.

143, 5569–5591. 10.1021/jacs.0c13388.

23. Leigh, D. A. Non-equilibrium structure and dynamics—Giving chemistry direction. (2023) Solvay Conference on Chemistry. In press.
24. Astumian, R. D., Chock, P. B., Tsong, T. Y., and Westerhoff, H. V. (1989). Effects of oscillations and energy-driven fluctuations on the dynamics of enzyme catalysis and free-energy transduction. Phys. Rev. A *39*, 6416–6435. 10.1103/physreva.39.6416.
25. Astumian, R. D., and Bier, M. (1996). Mechanochemical coupling of the motion of molecular motors to ATP hydrolysis. Biophys. Chem. *70*, 637–653. 10.1016/S0006-3495(96)79605-4.
26. Astumian, R. D. (1997). Thermodynamics and kinetics of a Brownian motor. Science *276*, 917–922. 10.1126/science.276.5314.917
27. Goldup, S., and Aprahamian, I. (2022). Off detailed balance: non-equilibrium steady states in catalysis, molecular motors and supramolecular materials. Preprint at ChemrXiv, 10.26434/chemrxiv-2022-49s4d-v2.
28. Das, K., Gabrielli, L., and Prins, L. J. (2021). Chemically fueled self-assembly in biology and chemistry. Angew. Chem. Int. Ed. *60*, 20120–20143. 10.1002/anie.202100274.
29. Amano, S., Esposito, M., Kreidt, E., Leigh, D. A., Penocchio, E., and Roberts, B. M. W. (2022). Using catalysis to drive chemistry away from equilibrium: relating kinetic asymmetry, power strokes, and the Curtin-Hammett principle in Brownian ratchets. J. Am. Chem. Soc. *144*, 20153−20164. 10.1021/jacs.2c08723.
30. Seeman, J. I. (1983). Effect of conformational change on reactivity in organic chemistry. Evaluations, applications, and extensions of Curtin–Hammett Winstein–Holness kinetics. Chem. Rev. *83*, 83–134. 10.1021/cr00054a001.
31. Seeman, J. I. (1986). The Curtin–Hammett principle and the Winstein–Holness equation: new definition and recent extensions to classical concepts. J. Chem. Educ. *63*, 42–48. 10.1021/ed063p42.
32. Amano, S., Esposito, M., Kreidt, E., Leigh, D. A., Penocchio, E., and Roberts, B. M. W. (2022). Insights from an information thermodynamics analysis of a synthetic molecular motor. Nat. Chem. *14*, 530–537. 10.1038/s41557-022-00899-z.
33. Parrondo, J. M. R., Horowitz, J. M., and Sagawa, T. (2015). Thermodynamics of information. Nat. Phys. *11*, 131–139. 10.1038/nphys3230.
34. Horowitz, J. M., and Esposito, M. (2014). Thermodynamics with continuous information flow. Phys. Rev. X *4*, 031015. 10.1103/PhysRevX.4.031015.
35. Ehrich, J., and Sivak, D. A. (2022). Energy and information flows in autonomous systems. Preprint at arXiv, 10.48550/arXiv.2209.10644.
36. Kassem, S., van Leeuwen, T., Lubbe, A. S., Wilson, M. R., Feringa, B. L., and Leigh, D. A. (2017). Artificial molecular motors. Chem. Soc. Rev. *46*, 2592–2621. 10.1039/C7CS00245A.
37. Kelly, T. R., De Silva, H., and Silva, R. A. (1999). Unidirectional rotary motion in a molecular system. Nature *401*, 150–152. 10.1038/43639.
38. Koumura, N., Zijlstra, R. W. J., van Delden, R. A., Harada, N., and Feringa, B. L. (1999). Light-driven monodirectional molecular rotor. Nature *401*, 152–155. 10.1038/43646.
39. Leigh, D. A., Wong, J. K. Y., Dehez, F., and Zerbetto, F. (2003). Unidirectional rotation in a mechanically interlocked molecular rotor. Nature *424*, 174–179. 10.1038/nature01758.
40. Fletcher, S. P., Dumur, F., Pollard, M. M., and Feringa, B. L. (2005). A reversible, unidirectional molecular rotary motor driven by chemical energy. Science *310*, 80–82. 10.1126/science.1117090.
41. Collins, B. S. L., Kistemaker, J. C. M., Otten, E., and Feringa, B. L. (2016). A chemically powered unidirectional rotary molecular motor based on a palladium redox cycle. Nat. Chem. *8*, 860–866. 10.1038/nchem.2543.
42. Wilson, M. R., Solà, J., Carlone, A., Goldup, S. M., Lebrasseur, N., and Leigh, D. A. (2016). An autonomous chemically fuelled small-molecule motor. Nature *534*, 235–240. 10.1038/nature18013.
43. Erbas-Cakmak, S., Fielden, S. D. P., Karaca, U., Leigh, D. A., McTernan, C. T., Tetlow, D. J., and Wilson, M. R. (2017). Rotary and linear molecular motors driven by pulses of a chemical fuel. Science *358*, 340–343. 10.1126/science.aao1377.
44. Zhang, Y., Chang, Z., Zhao, H., Crespi, S., Feringa, B. L., and Zhao, D. (2020). A chemically driven rotary molecular motor based on reversible lactone formation with perfect

unidirectionality. Chem *6*, 2420–2429. 10.1016/j.chempr.2020.07.025.

45. Borsley, S., Kreidt, E., Leigh, D. A., and Roberts, B. M. W. (2022). Autonomous fuelled directional rotation about a covalent single bond. Nature *604*, 80–85. 10.1038/s41586-022-04450-5.
46. Qiu, Y., Feng, Y., Guo, Q.-H., Astumian, R. D., and Stoddart, J. F. (2020). Pumps through the ages. Chem *6*, 1952–1977. 10.1016/j.chempr.2020.07.009.
47. Steinberg-Yfrach, G., Liddell, P. A., Hung, S.-C., Moore, A. L., Gust, D., and Moore, T. A., (1997). Conversion of light energy to proton potential in liposomes by artificial photosynthetic reaction centres. Nature *385*, 239–241. 10.1038/385239a0.
48. Bennett, I. M., Vanegas Farfano, H. M., Bogani, F., Primak, A., Liddell, P. A., Otero, L., Sereno, L., Silber, J. J., Moore, A. L., Moore, T. A., and Gust, D. (2002). Active transport of Ca^{2+} by an artificial photosynthetic membrane. Nature *420*, 398–401. 10.1038/nature01209.
49. Cheng, C., McGonigal, P. R., Schneebeli, S. T., Li, H., Vermeulen, N. A., Ke, C., and Stoddart, J. F. (2015). An artificial molecular pump. Nat. Nanotechnol. *10*, 547–553. 10.1038/nnano.2015.96.
50. Pezzato, C., Nguyen, M. T., Cheng, C., Kim, D. J., Otley, M. T., and Stoddart, J. F. (2017). An efficient artificial molecular pump. Tetrahedron *73*, 4849–4857. 10.1016/j.tet.2017.05.087.
51. Qiu, Y., Song, B., Pezzato, C., Shen, D., Liu, W., Zhang, L., Feng, Y., Guo, Q.-H., Cai, K., Li, W., Chen, H., Nguyen, M. T., Shi, Y., Cheng, C., Astumian, R. D., Li, X., and Stoddart, J. F. (2020). A precise polyrotaxane synthesizer. Science *368*, 1247–1253. 10.1126/science.abb3962.
52. Borsley, S., Leigh, D. A., and Roberts, B. M. W. (2021). A doubly kinetically-gated information ratchet autonomously driven by carbodiimide hydration. J. Am. Chem. Soc. *143*, 4414–4420. 10.1021/jacs.1c01172.
53. Amano, S. Fielden, S. D. P., and Leigh, D. A. (2021). A catalysis-driven artificial molecular pump. Nature *594*, 529–534. 10.1038/s41586-021-03575-3.
54. Liu, E., Cherraben, S., Boulo, L., Troufflard, C., Hasenknopf, B., Vives, G., and Sollogoub, M. (2023). A molecular information ratchet using a cone-shaped macrocycle. *Chem* published online 19 January 2023. 10.1016/j.chempr.2022.12.017
55. Feng, L., Qiu, Y., Guo, Q.-H., Chen, Z., Seale, J. S. W., He, K., Wu, H., Feng, Y., Farha, O. K., Astumian, R. D., and Stoddart, J. F. (2021). Active mechanisorption driven by pumping cassettes. Science *374*, 1215–1221. 10.1126/science.abk1391.
56. Thomas, D., Tetlow, D. J., Ren, Y., Kassem, S., Karaca, U., and Leigh, D. A. (2022). Pumping between phases with a pulsed-fuel molecular ratchet. Nat. Nanotechnol. *17*, 701–707. 10.1038/s41565-022-01097-1.
57. Borsley, S., Leigh, D. A., Roberts, B. M. W., and Vitorica-Yrezabal, I. J. (2022). Tuning the force, speed, and efficiency of an autonomous chemically fueled information ratchet. J. Am. Chem. Soc. *144*, 17241–17248. 10.1021/jacs.2c07633.
58. Seifert, U. (2012). Stochastic thermodynamics, fluctuation theorems and molecular machines. Rep. Prog. Phys. *75*, 126001. 10.1088/0034-4885/75/12/126001.
59. Corra, S., Bakić, M. T., Groppi, J., Baroncini, M., Silvi, S., Penocchio, E., Esposito, M., and Credi, A. (2022). Kinetic and energetic insights into the dissipative non-equilibrium operation of an autonomous light-powered supramolecular pump. Nat. Nanotechnol. *17*, 746–751. 10.1038/s41565-022-01151-y.
60. Ragazzon, G., Malferrari, M., Arduini, A., Secchi, A., Rapino, S., Silvi, S., and Credi, A. (2022). Autonomous non-equilibrium self-assembly and molecular movements powered by electrical energy. Angew. Chem. Int. Ed. e202214265. 10.1002/anie.202214265.
61. Leighton, M. P., and Sivak, D. A. (2022). Inferring subsystem efficiencies in bipartite molecular machines. Preprint at arXiv, 10.48550/arXiv.2209.12084.
62. Brouwer, A. M., Frochot, C., Gatti, F. G., Leigh, D. A., Mottier, L., Paolucci, F., Roffia, S., and Wurpel, G. W. H. (2001). Photoinduction of fast, reversible translational motion in a hydrogen-bonded molecular shuttle. Science *291*, 2124–2128. 10.1126/science.1057886.
63. Altieri, A., Gatti, F. G., Kay, E. R., Leigh, D. A., Martel, D., Paolucci, F., Slawin, A. M. Z., and Wong, J. K. Y. (2003) Electrochemically switchable hydrogen-bonded molecular

shuttles. J. Am. Chem. Soc. *125*, 8644–8654. 10.1021/ja0352552

64. Marlin, D. S., Cabrera, D. G. Leigh, D. A., and Slawin, A. M. Z. (2006). An allosterically regulated molecular shuttle. Angew. Chem. Int. Ed. *45*, 1385–1390. 10.1002/anie.200502624.
65. Tena-Solsona, M., Rieß, B., Grötsch, R. K., Löhrer, F. C., Wanzke, C., Käsdorf, B., Bausch, A. R., Müller-Buschbaum, P., Lieleg, O., and Boekhoven, J. (2017). Non-equilibrium dissipative supramolecular materials with a tunable lifetime. Nat. Commun. *8*, 15895. 10.1038/ncomms15895.
66. Kariyawasam, L. S., and Hartley, S. C. (2017). Dissipative assembly of aqueous carboxylic acid anhydrides fueled by carbodiimides. J. Am. Chem. Soc. *139*, 11949–11955. 10.1021/jacs.7b06099.
67. Kariyawasam, L. S., Hossain, M. M., and Hartley, S. C. (2020). The transient covalent bond in abiotic nonequilibrium systems. Angew. Chem. Int. Ed. *133*, 12756–12766. 10.1002/ange.202014678.
68. Rieß, B., Grötsch, R., and Boekhoven, J. (2020). The design of dissipative molecular assemblies driven by chemical reaction cycles. Chem *6*, 552–578. 10.1016/j.chempr.2019.11.008.
69. Schwarz, P., Tena Solsona, M., Dai, K., and Boekhoven, J. (2021). Carbodiimide-fueled catalytic reaction cycles to regulate supramolecular processes. Chem. Commun. *58*, 1284–1297. 10.1039/D1CC06428B.
70. Schnitter, F., and Boekhoven, J. (2021). A method to quench carbodiimide-fueled self-assembly. ChemSystemsChem *3*, e200003. 10.1002/syst.202000037.
71. Fisher, M. E., and Kolomeisky, A. B. (1999). The force exerted by a molecular motor. Proc. Natl. Acad. Sci. U. S. A. *96*, 6597–6602. 10.1073/pnas.96.12.6597.
72. Shibata, T., and Fujimoto, K. (2004). Noisy signal amplification in ultrasensitive signal transduction. Proc. Natl. Acad. Sci. U. S. A. *102*, 331–336. 10.1073/pnas.0403350102.
73. Cheong, R., Rhee, A., Wang, C. J., Nemenman, I., and Levchenko, A. (2011). Information transduction capacity of noisy biochemical signaling networks. Science *334*, 354–358. 10.1126/science.1204553.
74. Ito, S., and Sagawa, T. (2015). Maxwell's demon in biochemical signal transduction with feedback loop. Nat. Commun. *6*, 7498. 10.1038/ncomms8498.
75. Bialek, W., and Setayeshgar, S. (2005). Physical limits to biochemical signaling. Proc. Nat. Acad. Sci. *102*, 10040–10045. 10.1073/pnas.0504321102.
76. Berg, H. C., and Purcell, E. M. (1977). Physics of chemoreception. Biophys. J. *20*, 193–219. 10.1016/S0006-3495(77)85544-6.
77. Ragazzon, G., and Prins, L. J. (2018). Energy consumption in chemical fuel-driven self-assembly. Nat. Nanotechnol. *13*, 882–889. 10.1038/s41565-018-0250-8.
78. Penocchio, E., and Ragazzon, G. (2022). Kinetic asymmetry profiles as a holistic approach to engineer molecular non-equilibrium systems. Small 2206188. 10.1002/smll.202206188.
79. Di Noja, S., Garrido, M., Gualandi, L., and Ragazzon, G. (2023). Control over dethreading kinetics allows evaluating the entropy stored in an interlocked molecular machine out-of-equilibrium. Angew. Chem. Int. Ed. e202300295. 10.1002/chem.202300295.
80. Rao, R., and Esposito, M. (2016). Nonequilibrium thermodynamics of chemical reaction networks: wisdom from stochastic thermodynamics. Phys. Rev. X *6*, 041064. 10.1103/PhysRevX.6.041064.
81. Penocchio, E., Rao, R., and Esposito, M. (2019). Thermodynamic efficiency in dissipative chemistry. Nat. Commun. *10*, 3865. 10.1038/s41467-019-11676-x.
82. Cover, T. M., and Thomas, J. A. (2012) Elements of Information Theory (Wiley).
83. Lathouwers, E., and Sivak, D. A. (2022). Internal energy and information flows mediate input and output power in bipartite molecular machines. Phys. Rev. E *105*, 024136. 10.1103/PhysRevE.105.024136.
84. Penocchio, E., Avanzini, F., and Esposito, M. (2022). Information thermodynamics for deterministic chemical reaction networks. J. Chem. Phys. *157*, 034110. 10.1063/5.0094849.
85. Leff, H. S., and Rex, A. F. (1990). Maxwell's Demon: Entropy, Information, Computing (Princeton University Press).
86. Freitas, N., and Esposito, M. (2021). Characterizing autonomous Maxwell demons.

Phys. Rev. E *103*, 032118. 10.1103/PhysRevE.103.032118.

87. Zhang, Y., Giżyński, K., Maciołek, A., and Hołyst, R. (2020). Storage of energy in constrained non-equilibrium systems. Entropy *22*, 557. 10.3390/e22050557.
88. Saha, T. K., Lucero, J. N. E., Ehrich, J., Sivak, D. A., and Bechhoefer, J. (2021). Maximizing power and velocity of an information engine. Proc. Natl. Acad. Sci. U. S. A. *118*, e2023356118. 10.1073/pnas.2023356118.
89. Tu, Y. (2008). The nonequilibrium mechanism for ultrasensitivity in a biological switch: sensing by Maxwell's demons. Proc. Natl. Acad. Sci. U. S. A. *105*, 11737–11741. 10.1073/pnas.0804641105.
90. Hartich, D., Barato, A. C., and Seifert, U. (2015). Nonequilibrium sensing and its analogy to kinetic proofreading. New. J. Phys. *17*, 055026. 10.1088/1367-2630/17/5/055026.
91. Tkačik, G., and Bialek, W. (2016). Information processing in living systems. Annu. Rev. Condens. Matter Phys. *7*, 89–117. 10.1146/annurev-conmatphys-031214-014803.
92. Boël, G., Danot, O., de Lorenzo, V., and Danchin, A. (2019). Omnipresent Maxwell's demons orchestrate information management in living cells. Microb. Biotechnol. *12*, 210–242. 10.1111/1751-7915.13378.
93. Mizraji, E. (2021). The biological Maxwell's demons: exploring ideas about the information processing in biological systems. Theory Biosci. *140*, 307–318. 10.1007/s12064-021-00354-6.
94. Efremov, A., and Wang, Z. (2011). Universal optimal working cycles of molecular motors. Phys. Chem. Chem. Phys. *13*, 6223–6233. 10.1039/c0cp02118k.
95. Wagoner, J. A., and Dill, K. A. (2019). Opposing pressures of speed and efficiency guide the evolution of molecular machines. Mol. Biol. Evol. *36*, 2813–2822. 10.1093/molbev/msz190.
96. Wagoner, J. A., and Dill, K. A. (2019). Mechanisms for achieving high speed and efficiency in biomolecular machines. Proc. Natl. Acad. Sci. U. S. A. *116*, 5902–5907. 10.1073/pnas.1812149116.
97. Gupta, D., Large, S. J., Toyabe, S., and Sivak, D. A. (2022). Optimal control of the F_1-ATPase molecular motor. J. Phys. Chem. Lett. *13*, 11844–11849. 10.1021/acs.jpclett.2c03033.
98. Lutz, E., and Ciliberto, S. (2015). Information: From Maxwell's demon to Landauer's eraser. Phys. Today *68*, 30. 10.1063/PT.3.2912.